Editors' Suggestion

Final SeaQuest Results on the Flavor Asymmetry of the Proton Light-Quark Sea with Proton-Induced Drell-Yan Process

C. H. Leung,[1,*,†] J. Dove,[1] K. Nagai,[2,3,4,5] K. Nakano,[6,7] S. Prasad,[1,8] A. S. Tadepalli,[9,†] C. A. Aidala,[10,2] J. Arrington,[8,‡] C. Ayuso,[10] C. L. Barker,[11] W. C. Chang,[3] A. Chen,[1] D. C. Christian,[12] B. P. Dannowitz,[1] L. El Fassi,[13,9] D. F. Geesaman,[8] R. Gilman,[9] Y. Goto,[7] R. S. Guo,[14] L. Guo,[2,§] T. J. Hague,[11,†] R. J. Holt,[8,‖] M. F. Hossain,[15,6] L. D. Isenhower,[11] E. R. Kinney,[16] A. Klein,[2] D. Kleinjan,[2] P.-J. Lin,[16,3,17] K. Liu,[2] M. X. Liu,[2] W. Lorenzon,[10] R. E. McClellan,[1,¶] P. L. McGaughey,[2] M. M. Medeiros,[8] Y. Miyachi,[18] S. Miyasaka,[4] D. H. Morton,[10] K. Nakahara,[19] J. C. Peng,[1] A. J. R. Puckett,[2,**] A. Pun,[15] B. J. Ramson,[10] P. E. Reimer,[8] J. G. Rubin,[8,10] F. Sanftl,[4] S. Sawada,[20] T. Sawada,[10] M. B. C. Scott,[10,8,††] T.-A. Shibata,[4,7,‡‡] D.-S. Su,[3] M. Teo,[1] R. Towell,[11] S. Uemura,[2,§§] S. G. Wang,[3,14,12,‖‖] J. Wu,[12] N. Wuerfel,[10] and Z. H. Ye[8,¶¶]

(FNAL E906/SeaQuest Collaboration)

[1]*Department of Physics, University of Illinois at Urbana-Champaign, Urbana, Illinois 61801, USA*
[2]*Los Alamos National Laboratory, Los Alamos, New Mexico 87545, USA*
[3]*Institute of Physics, Academia Sinica, Taipei 11529, Taiwan*
[4]*Department of Physics, Tokyo Institute of Technology, Meguro-ku, Tokyo 152-8550, Japan*
[5]*Department of Physics and Materials Science, The University of Memphis, Memphis, Tennessee 38152, USA*
[6]*University of Virginia, Charlottesville, Virginia 22904, USA*
[7]*RIKEN Nishina Center for Accelerator-Based Science, Wako, Saitama 351-0198, Japan*
[8]*Physics Division, Argonne National Laboratory, Lemont, Illinois 60439, USA*
[9]*Department of Physics and Astronomy, Rutgers, The State University of New Jersey, Piscataway, New Jersey 08854, USA*
[10]*Randall Laboratory of Physics, University of Michigan, Ann Arbor, Michigan 48109, USA*
[11]*Department of Engineering and Physics, Abilene Christian University, Abilene, Texas 79699, USA*
[12]*Fermi National Accelerator Laboratory, Batavia, Illinois 60510, USA*
[13]*Department of Physics and Astronomy, Mississippi State University, Mississippi State, Mississippi 39762, USA*
[14]*Department of Physics, National Kaohsiung Normal University, Kaohsiung 824, Taiwan*
[15]*Department of Physics, New Mexico State University, Las Cruces, New Mexico 88003, USA*
[16]*Department of Physics, University of Colorado, Boulder, Colorado 80309, USA*
[17]*Department of Physics, National Central University, Jhongli District, Taoyuan City 32001, Taiwan*
[18]*Department of Physics, Yamagata University, Yamagata City, Yamagata 990-8560, Japan*
[19]*Department of Physics, University of Maryland, College Park, Maryland 20742, USA*
[20]*Institute of Particle and Nuclear Studies, KEK, High Energy Accelerator Research Organization, Tsukuba, Ibaraki 305-0801, Japan*

(Received 8 January 2026; revised 6 March 2026; accepted 17 March 2026; published 30 April 2026)

[*]Contact author: cleung@jlab.org
[†]Present address: Thomas Jefferson National Accelerator Facility, Newport News, Virginia 23606, USA.
[‡]Present address: Lawrence Berkeley National Laboratory, Berkeley, California 94720 USA.
[§]Present address: Physics Department, Florida International University, Miami, Florida, 33199, USA.
[‖]Present address: Kellogg Radiation Laboratory, California Institute of Technology, Pasadena, California 91125, USA.
[¶]Present address: Pensacola State College, Pensacola, Florida 32504, USA.
[**]Present address: University of Connecticut, Storrs, Connecticut 06269, USA.
[††]Present address: George Washington University, Washington, DC 20052, USA.
[‡‡]Present address: Nihon University, College of Science and Technology, Chiyoda-ku, Tokyo 101-8308, Japan.
[§§]Present address: Fermi National Accelerator Laboratory, Batavia, Illinois 60510, USA.
[‖‖]Present address: APS, Argonne National Laboratory, Lemont, Illinois 60439, USA.
[¶¶]Present address: Department of Physics, Tsinghua University, Beijing 100084, China.

The Fermilab E906/SeaQuest collaboration performed measurements of the Drell-Yan process using 120 GeV proton beams bombarding liquid hydrogen and liquid deuterium targets. A combined analysis of all collected data was performed to obtain the final results for the $\sigma_{pd}/2\sigma_{pp}$ Drell-Yan cross section ratio covering the kinematic region of $0.13 < x < 0.45$. The x dependencies of $\bar{d}(x)/\bar{u}(x)$ and $\bar{d}(x) - \bar{u}(x)$ are extracted from these cross section ratios. It is found that $\bar{d}(x)$ is greater than $\bar{u}(x)$ over the entire measured x range, with improved statistical accuracy compared to previous measurements. The new results on $\bar{d}(x)/\bar{u}(x)$ and $\bar{d}(x) - \bar{u}(x)$ are compared to various parton distribution functions and theoretical calculations.

DOI: 10.1103/fdrg-gw3s

Following the discovery of the pointlike constituents in the proton in deep-inelastic scattering (DIS) experiments, evidence for a nucleon sea, made of quark-antiquark pairs, was revealed from the observation of the sharp rise of the structure functions as $x \to 0$. In contrast to the situation for atoms, where the particle-antiparticle pairs play a relatively minor role, the quark-antiquark pairs in the nucleon form an integral part for depicting the internal structure of hadrons, owing to the large coupling strength α_s in strong interactions [1].

The earliest parton models assumed that the proton sea was SU(2) flavor symmetric, even though the proton's valence quark distributions are not flavor symmetric. This flavor symmetry assumption for the proton sea was not based on any known physics; instead, it reflected the expectation from perturbative QCD that the splitting of gluons into quark-antiquark pairs should be nearly up-down flavor symmetric due to the comparable masses for the up and down quarks.

Evidence for the asymmetry of the $\bar{u}$ and $\bar{d}$ sea-quark distributions in the proton was first found in deep-inelastic scattering experiments [2–4] via the observation of the violation of the Gottfried Sum Rule [5]. Field and Feynman attributed the asymmetry observed in the early SLAC DIS data to the Pauli Exclusion Principle [6]. Many theoretical models have been proposed to explain the asymmetry, including the meson-cloud model [7,8], which already predicted the asymmetry in 1982; the chiral-quark model [9]; and the statistical model [10,11]. It was pointed out [12] that an independent experimental technique to probe this flavor asymmetry is to measure the Drell-Yan cross section ratios, $\sigma_{pd}/2\sigma_{pp}$, which can further determine the x dependence of this flavor asymmetry.

The Drell-Yan cross section ratios, $\sigma_{pd}/2\sigma_{pp}$, have been measured by the CERN NA51 experiment at 400 GeV for a single value of x [13] and by the FNAL E866/NuSea experiment for the $0.015 < x < 0.35$ region with an 800 GeV proton beam [14–16]. Subsequent measurements by the HERMES collaboration, using the semi-inclusive DIS reaction [17], and by the STAR collaboration, using W-boson production in $p + p$ collisions, gave further confirmation of the up-down sea-quark flavor asymmetry in the small x region. The surprisingly large flavor asymmetry of the nucleon sea has inspired much theoretical work, as discussed in several review articles [18–22].

While the small x region of the sea-quark flavor asymmetry was accurately measured by the FNAL E866/NuSea experiment, the highest x data points from E866 suggest a possible reversal of the sea-quark flavor asymmetry for $x > 0.25$, but with large statistical uncertainties. A new measurement with improved accuracy for the large x region was clearly warranted. The FNAL E906/SeaQuest experiment, using a new spectrometer [23] and a 120 GeV proton beam, was performed to shed new light on the flavor asymmetry of the proton at the large x region.

Results from the analysis of the first part of the SeaQuest data, corresponding to roughly half of the total data collected in the experiment, have been reported in earlier publications [24,25]. These analyses, adopting two different methods, showed that the $\sigma_{pd}/2\sigma_{pp}$ Drell-Yan cross section ratios remain above unity, implying that $\bar{d}$ is greater than $\bar{u}$ for the entire x range measured at SeaQuest. Results on the $\sigma_{pd}/2\sigma_{pp}$ cross section ratios for charmonium production, reported recently in Ref. [26], are also consistent with the flavor asymmetry deduced from the Drell-Yan data. Several recent global parton distribution function (PDF) analyses [27–31] have included these results, in addition to the W-boson production data from the STAR collaboration [32], to better constrain the flavor asymmetry of $\bar{u}$ and $\bar{d}$ in the proton. The SeaQuest flavor asymmetry data have also been compared with the predictions from the statistical model [33], the pion-cloud model [34], and the Pauli blocking effect [35,36].

In this Letter we present the final results on Drell-Yan $\sigma_{pd}/2\sigma_{pp}$ ratios from the SeaQuest experiment, including all data collected during the run periods of June 2014–July 2015 and March 2016–July 2017. The combined dataset contains roughly twice as many detected muons as in our previous publications. Because the trigger conditions and detector configuration differed between the two running periods, we analyzed each dataset separately. Results from the two datasets were first compared for consistency and then combined to produce the final results.

The SeaQuest experiment detects $\mu^+\mu^-$ pairs (dimuons) produced in the interaction of a proton beam with various target nuclei. The production of massive dimuon pairs is

described by the Drell-Yan process [37] with the leading order cross section given as

$$\frac{d^2\sigma}{dx_1 dx_2} = \frac{4\pi\alpha^2}{9x_1x_2s} \times \sum_{i\in u,d,s,\ldots} e_i^2[q_i^A(x_1)\bar{q}_i^B(x_2) + \bar{q}_i^A(x_1)q_i^B(x_2)], \quad (1)$$

where α is the fine-structure constant, s is the center-of-mass energy squared, e_i is the charge of a quark with flavor i, and $q_i^{A,B}(x_{1,2})$ are the quark distribution functions in hadrons A and B for quarks carrying a momentum fraction x_1 and x_2, respectively. The variables x_1 and x_2 of the quark-antiquark pair are calculated from the four-momentum Q of virtual photon,

$$x_1 = \frac{P_2 \cdot Q}{P_2 \cdot (P_1 + P_2)}, \quad \text{and} \quad x_2 = \frac{P_1 \cdot Q}{P_1 \cdot (P_1 + P_2)}, \quad (2)$$

where P_1 and P_2 are the four momenta of the projectile and target hadron, respectively. An analogous notation is used for antiquark distribution functions $\bar{q}_i^{A,B}(x_{1,2})$. For fixed-target experiments like SeaQuest, the spectrometers have large acceptance only for the positive x_F $[x_F = 2p_L/\sqrt{s}(1 - M^2/s)]$ region, where p_L is the longitudinal momentum of the dimuon in the hadron-hadron center-of-mass frame and M is the dimuon mass. Thus, the Drell-Yan cross section is dominated by the first term in Eq. (1), corresponding to the annihilation of a beam quark with a target antiquark. Assuming $\sigma^{pd} \approx \sigma^{pp} + \sigma^{pn}$, which neglects small nuclear effects of the deuteron [18,38], and charge symmetry for the parton distributions [39], Eq. (1) yields the following approximation for the target ratio:

$$\frac{\sigma^{pd}}{2\sigma^{pp}} \approx \frac{1}{2}\frac{4 + \frac{d(x_1)}{u(x_1)}}{4 + \frac{d(x_1)}{u(x_1)}\frac{\bar{d}(x_2)}{\bar{u}(x_2)}}\left[1 + \frac{\bar{d}(x_2)}{\bar{u}(x_2)}\right] \approx \frac{1}{2}\left[1 + \frac{\bar{d}(x_2)}{\bar{u}(x_2)}\right]. \quad (3)$$

While Eq. (3) illustrates the power of the $\sigma^{pd}/2\sigma^{pp}$ Drell-Yan cross section ratio to reveal the flavor asymmetry between $\bar{d}$ and $\bar{u}$, the actual extraction of the $\bar{d}(x)/\bar{u}(x)$ ratios from the measured $\sigma^{pd}/2\sigma^{pp}$ Drell-Yan cross section ratios is performed using a Next-to-Leading Order (NLO) calculation.

The SeaQuest spectrometer is described in detail in Ref. [23]. The experiment receives the proton beam from the Fermilab Main Injector at 120 GeV once every minute in four-second periods (spills), with an average intensity of 6×10^{12} protons per spill. The target system consists of two liquid targets (hydrogen and deuterium), three solid targets (iron, carbon, and tungsten), and two calibration targets ("empty flask" and "no target"). A solid iron magnet focuses the high-mass dimuons into the spectrometer. The spectrometer consists of four tracking stations, with an open-air magnet between stations 1 and 2. Each tracking station consists of hodoscope planes, which provide fast signals for triggering, and drift chambers or proportional tubes, which provide precise position information for tracking. The main physics trigger requires a coincidence of two opposite-sign muons, one in the top half and one in the bottom half of the spectrometer. A separate trigger only requires one muon track, and it is mainly used for studying the accidental background.

The muon tracks are reconstructed using the hits in the drift chambers and proportional tubes in each station. After identifying hits potentially originating from interactions within the target region, the Kalman filter algorithm [40] is used to reconstruct the muon tracks. A Kalman filter algorithm [40] is used to reconstruct muon trajectories and momenta from hits in the drift chambers and proportional tubes. Hits originating in the target region are first selected; the Kalman filter is then applied to determine the best-fit tracks and the interaction vertex. A detailed description of the analysis procedure can be found in earlier publications [24,25].

A GEANT4 [41–43] based Monte Carlo simulation has been developed to compare data with expectations. The Drell-Yan events are generated with the dimuon mass and x_F distributions obtained with the CT14 nucleon PDFs [44]. The dimuon transverse momentum distribution is adjusted to match the measured distribution [45,46]. The efficiency and the resolution of the chambers are taken into account in the simulation. An embedding procedure has also been developed to simulate the background hits by embedding each Monte Carlo event with hits recorded by the random trigger [47].

The dimuon mass spectrum, as shown in Fig. 1 for data collected on the liquid hydrogen target for the second part

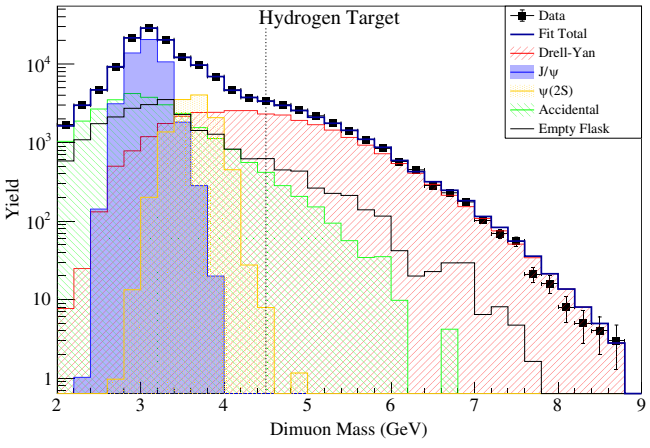

FIG. 1. Dimuon mass distribution for events collected on the liquid hydrogen target for the second dataset. The data points (solid squares) are compared with a fit consisting of various components (see text).

of the experiment, consists of various components including the Drell-Yan process, the charmonium production, accidental background, and other background sources. These different components often have distinct mass spectra; for example, the J/ψ and $\psi(2S)$ decays would have sharp distributions centered around their masses. Therefore, the data can be fitted to various templates to obtain the relative contribution from each source. As input parameters to the fit, the mass distributions for J/ψ, $\psi(2S)$ and the Drell-Yan are obtained from studying the Monte Carlo simulation. The mass distribution of accidental coincidence events was made by pairing at random μ^+ and μ^- collected with the "single-muon" trigger under the condition that the beam intensities of μ^+ and μ^- events were comparable. An empty-flask target, which consists of a vacuum filled target flask, is used to measure the background from interactions of the beam with materials other than the target, such as the target flask itself and the beam dump. The magnitudes of these components, with the exception of the empty-flask data for which the normalization is known, were varied in the fit to the mass spectrum. The statistical uncertainties of the Monte Carlo and empty-flask data are taken into account using the algorithm described in Ref. [48]. Figure 1 shows the fit to the $p+p$ dimuon spectrum, and the mass distribution is well described by this fitting procedure.

After the mass fit is performed, a mass cut ($M > 4.5$ GeV) is applied to remove the J/ψ and $\psi(2S)$ events. The remaining events are projected into various kinematic variables, such as x_1, x_2, and x_F. The accidental background and empty-flask contributions are then subtracted from the data. Several corrections are applied to extract the final Drell-Yan yields. These include the dead time correction for the effective luminosity, and a target contamination correction is also applied to the D_2 data due to H contamination in the target cell. The reconstruction inefficiency and data acquisition system dead time, which have a small but non-negligible target dependence, are also taken into account. For this analysis, a revised target contamination correction is used, as compared with the earlier work [24,25], resulting in a roughly 2% upward shift in the measured cross section ratios.

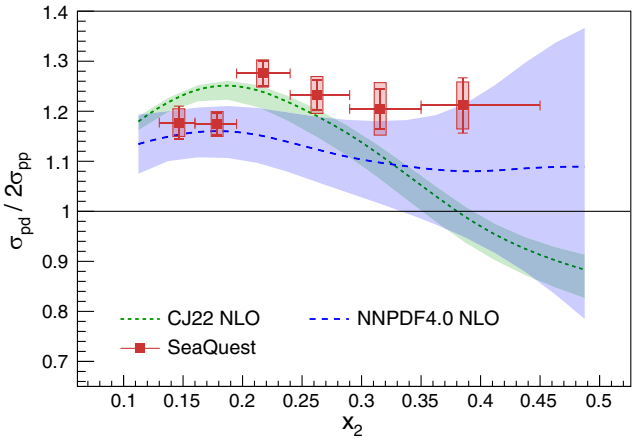

FIG. 2. Measured $\sigma_{pd}/2\sigma_{pp}$ Drell-Yan cross section ratio from SeaQuest compared calculations using CJ22 [29] and NNPDF4.0 [28]. The error bands on the theoretical calculations correspond to the 68% confidence level from the PDFs.

The $\sigma_{pd}/2\sigma_{pp}$ cross section ratios versus x_2 obtained from the analysis of the full SeaQuest dataset are shown in Fig. 2. The ratios as functions of other variables are shown in Fig. 4 in the End Matter. The main systematic uncertainties originate from modeling the accidental background (0.41%–3.82%). Different methods for generating the accidental background distributions have been studied [49] to estimate the uncertainty, and the differences are quoted as the systematic uncertainty. Other sources of systematic uncertainties include the efficiency corrections (0.46%–0.74%), the empty flask normalization (0.10%–0.16%), and the relative beam luminosity (2%).

The two datasets are analyzed separately and compared for consistency. The final results are obtained by taking an average, weighted by the inverse of the total uncertainty squared. A comparison of the two datasets is shown in Fig. 5 in the End Matter. Except for the smallest x_2 point, the results from the two datasets are in good agreement, with differences less than 1σ. The flavor asymmetry is very well constrained for the smallest x_2 bin by previous experiments, and the final result on the measured cross section at the smallest x_2 bin is in better agreement with

TABLE I. Measured $\sigma_{pd}/2\sigma_{pp}$ cross section ratio as well as the extracted $\bar{d}/\bar{u}$ and $\bar{d}-\bar{u}$ for each x_2 bin. The first uncertainty is statistical, and the second is systematic. The average values of kinematic variables in each x_2 bin are also shown.

x_2 range	$\langle x_2\rangle$	$\langle x_1\rangle$	$\langle p_T\rangle$ (GeV/c)	$\langle M\rangle$ (GeV/c^2)	$\sigma_{pd}/2\sigma_{pp}$	$\bar{d}/\bar{u}$	$\bar{d}-\bar{u}$
0.130–0.160	0.146	0.687	0.760	4.71	$1.177 \pm 0.033 \pm 0.028$	$1.383^{+0.058+0.060}_{-0.053-0.060}$	$0.176^{+0.021+0.024}_{-0.022-0.023}$
0.160–0.195	0.181	0.610	0.759	4.87	$1.174 \pm 0.022 \pm 0.025$	$1.431^{+0.041+0.061}_{-0.051-0.061}$	$0.111^{+0.011+0.011}_{-0.011-0.011}$
0.195–0.240	0.222	0.553	0.760	5.11	$1.275 \pm 0.024 \pm 0.027$	$1.672^{+0.052+0.082}_{-0.052-0.082}$	$0.092^{+0.012+0.012}_{-0.012-0.012}$
0.240–0.290	0.263	0.516	0.761	5.44	$1.232 \pm 0.029 \pm 0.037$	$1.653^{+0.073+0.123}_{-0.073-0.113}$	$0.043^{+0.003+0.013}_{-0.003-0.013}$
0.290–0.350	0.324	0.492	0.762	5.83	$1.205 \pm 0.040 \pm 0.052$	$1.694^{+0.124+0.174}_{-0.114-0.174}$	$0.024^{+0.004+0.004}_{-0.004-0.004}$
0.350–0.450	0.395	0.474	0.762	6.34	$1.212 \pm 0.055 \pm 0.047$	$1.925^{+0.205+0.205}_{-0.195-0.205}$	$0.015^{+0.005+0.005}_{-0.005-0.005}$

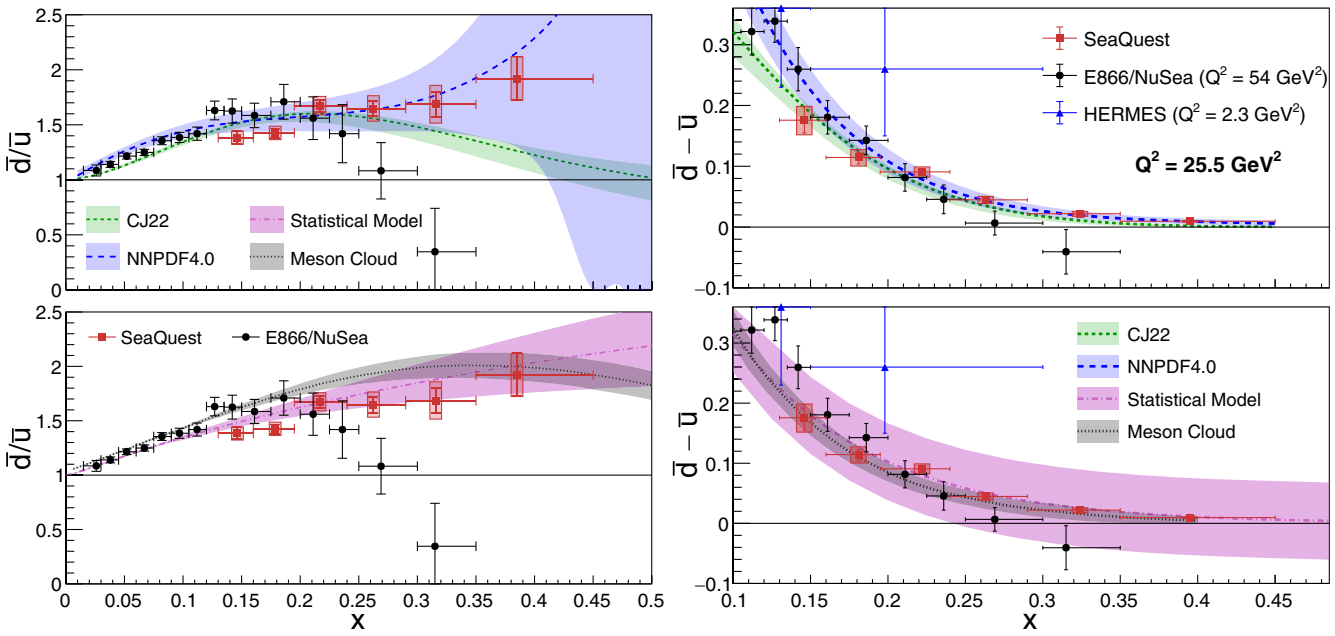

FIG. 3. Extracted $\bar{d}(x)/\bar{u}(x)$ (left) and $\bar{d}(x)-\bar{u}(x)$ (right) from the measured $\sigma_{pd}/2\sigma_{pp}$ Drell-Yan cross section ratio from SeaQuest (red squares), E866 [16] (black circles), and HERMES [17] (blue triangles). The extracted ratios are compared with CJ22 [29] and NNPDF4.0 [28] global PDF analyses (top) and with predictions from statistical model [33] and meson cloud model [34] (bottom). The error bands on the PDFs correspond to their 68% confidence level.

theoretical expectations than the individual datasets. The results are shown in Fig. 2 and tabulated in Table I. Figure 2 compares the SeaQuest results with NLO calculations using DYTurbo [50], with nucleon PDFs CJ22 [29] and NNPDF4.0 [28]. Both PDFs are obtained from global analyses including the earlier SeaQuest results [24]. This partly explains the better agreement between the data and the NNPDF4.0 calculation, although the data tend to lie above the calculation at large x. Nevertheless, Fig. 2 shows that both the data and the NNPDF4.0 calculation for the $\sigma_{pd}/2\sigma_{pp}$ cross section ratio exceed unity over the entire measured x region. With the increased statistics in the updated analysis, the constraint on the light sea-quark asymmetry in future global analyses can be further improved.

To facilitate comparison between the SeaQuest result and predictions from various models, the $\bar{d}(x)/\bar{u}(x)$ ratio is extracted from the cross section ratio using an iterative method described in Ref. [24]. We first estimate the $\bar{d}(x)/\bar{u}(x)$ ratio over the measured x_2 and calculate the cross section ratio R using a chosen PDF set. This PDF set provides all parton distributions including the $\bar{d}(x)+\bar{u}(x)$, except that the $\bar{d}(x)/\bar{u}(x)$ ratio is allowed to vary. The calculated cross section is weighted by the spectrometer acceptance, determined using Monte Carlo simulations. The acceptance is tabulated in Table IV. The cross section ratios R are then computed at next-to-leading order as functions of x_2 and compared with the data. The $\bar{d}(x)/\bar{u}(x)$ ratios are adjusted until the difference between data and calculation is less than 10^{-3}.

The extracted $\bar{d}(x)/\bar{u}(x)$ from the measured SeaQuest cross section ratio, using the CT18 PDFs as the basis, is shown in Fig. 3 and tabulated in Table I. While the SeaQuest results are consistent with previous E866 results [16] at low x, the extracted $\bar{d}(x)/\bar{u}(x)$ ratios from the SeaQuest measurement continue to rise as x increases and are in tension with the E866 result. The extracted $\bar{d}(x)/\bar{u}(x)$ ratios are compared with results from CJ22 [29] and NNPDF4.0 [28] global analyses in Fig. 3. NNPDF4.0 and the CJ22 global analyses, which both include the earlier SeaQuest results [24], both prefer $\bar{d}(x)/\bar{u}(x) > 1$ in the large x region covered by the SeaQuest measurement. With the improved statistical accuracy from the combined analysis presented in this Letter, the uncertainty on $\bar{d}(x)/\bar{u}(x)$ in these global analyses can be further reduced. The SeaQuest results are also in much better agreement with predictions from the meson cloud model [34] and the statistical model [33].

The isovector quantity $\bar{d}(x)-\bar{u}(x)$ is of interest since perturbative processes should not produce any significant difference between $\bar{d}(x)$ and $\bar{u}(x)$. Hence, $\bar{d}(x)-\bar{u}(x)$ can provide a direct measure of the nonperturbative contribution to the proton sea. From the $\bar{d}(x)/\bar{u}(x)$ ratios extracted from SeaQuest, we calculated $\bar{d}(x)-\bar{u}(x)$ by taking the $\bar{d}(x)+\bar{u}(x)$ values from the CT18 proton PDFs. The values of $\bar{d}(x)-\bar{u}(x)$ derived from the SeaQuest data are shown in Fig. 3 and tabulated in Table I, and they are compared with results from E866 [16] and HERMES [17]. The derived $\bar{d}(x)-\bar{u}(x)$ are also compared with

TABLE II. Values of $\int_{0.13}^{0.45}[\bar{d}(x)-\bar{u}(x)]\mathrm{d}x$ and $\int_{0.13}^{0.45}x[\bar{d}(x)-\bar{u}(x)]\mathrm{d}x$ at $Q^2=25.5$ GeV^2 extracted from SeaQuest compared with CJ22 [29] and NNPDF4.0 [28] PDFs as well as the statistical models [33] and the meson cloud [34].

		PDFs		Models	
	SeaQuest	CJ22	NNPDF4.0	Stat	Meson cloud
$\int_{0.13}^{0.45}[\bar{d}(x)-\bar{u}(x)]\mathrm{d}x$	$0.0179^{+0.0017\ +0.0022}_{-0.0018\ -0.0023}$	$0.0167^{+0.0009}_{-0.0028}$	$0.0208^{+0.0036}_{-0.0036}$	0.0186	0.0180
$\int_{0.13}^{0.45}x[\bar{d}(x)-\bar{u}(x)]\mathrm{d}x$	$0.00368^{+0.00034\ +0.00045}_{-0.00036\ -0.00049}$	$0.00319^{+0.00019}_{-0.00063}$	$0.00414^{+0.00078}_{-0.00078}$	0.00386	0.00361

predictions from the meson cloud and the statistical models in Fig. 3. Like the $\bar{d}(x)/\bar{u}(x)$ ratio, the deduced $\bar{d}-\bar{u}$ is also in good agreement with both models.

The SeaQuest data can also be used to calculate two integrals: $\int_{0.13}^{0.45}[\bar{d}(x)-\bar{u}(x)]\mathrm{d}x$, which describes the integrated sea-quark flavor asymmetry, and $\int_{0.13}^{0.45}x[\bar{d}(x)-\bar{u}(x)]\mathrm{d}x$, which represents the difference in the momentum fractions carried by $\bar{u}$ and $\bar{d}$ quarks. These values are listed in Table II and compared with different PDFs and models. The SeaQuest results are in good agreement with NNPDF4.0 and with the model predictions.

In summary, we have reported the improved results on the $\sigma_{pd}/2\sigma_{pp}$ Drell-Yan cross section ratio up to $x_2=0.45$, based on the analysis of the entire SeaQuest dataset, which supersedes the earlier results in Refs. [24,25]. The measured ratio remains above unity, which suggests that the $\bar{d}(x)/\bar{u}(x)$ ratio continues to increase at large x. The improved statistical precision presented in this Letter will help to further constrain the light sea-quark asymmetry in future global analyses. These results support the excess of $\bar{d}$ compared to $\bar{u}$ that is obtained in various model predictions, including the meson cloud model and the statistical model. With recent developments in lattice calculations within the framework of large momentum effective theory [51], these results can provide an important benchmark for future lattice calculations. With the advent of the Electron Ion Collider, the flavor asymmetry in the small x region, where abundant sea quarks reside, can be further measured via the semi-inclusive DIS reaction [17].

Acknowledgments—We thank the late G. T. Garvey for contributions to the early stages of this experiment, C. N. Brown for contributions to five decades of dimuon experiments at Fermilab, and N. C. R. Makins for contributions to the execution of the experiment. We also thank the Fermilab Accelerator Division and Particle Physics Division for their support of this experiment. This work was performed by the SeaQuest Collaboration, whose work was supported in part by the U.S. Department of Energy, Office of Nuclear Physics under Contract No. DE-AC02-06CH11357, Grants No. DE-FG02-03ER41243 and No. DE-FG02-07ER41528; the U.S. National Science Foundation under Grants No. PHY 2013002, No. PHY 2110229, No. PHY 2111046, No. PHY 2209348, No. PHY 2309922, and No. PHY 2514181; the JSPS (Japan) KAKENHI through Grants No. 21244028, No. 25247037, No. 25800133, No. 18H03694, No. 20K04000, No. 22H01244, No. 23K22515, and No. 25K07341; and the National Science and Technology Council of Taiwan (R. O. C.). Fermilab is managed by FermiForward Discovery Group, LLC, under Contract No. 89243024CSC000002.

Data availability—The data that support the findings of this article are openly available [52].

[1] J. I. Friedman and H. W. Kendall, Annu. Rev. Nucl. Sci. **22**, 203 (1972).
[2] S. Stein, W. B. Atwood, E. D. Bloom, R. L. A. Cottrell, H. DeStaebler, C. L. Jordan, H. G. Piel, C. Y. Prescott, R. Siemann, and R. E. Taylor, Phys. Rev. D **12**, 1884 (1975).
[3] P. Amaudruz *et al.* (New Muon Collaboration), Phys. Rev. Lett. **66**, 2712 (1991).
[4] M. Arneodo *et al.* (New Muon Collaboration), Phys. Rev. D **50**, R1 (1994).
[5] K. Gottfried, Phys. Rev. Lett. **18**, 1174 (1967).
[6] R. D. Field and R. P. Feynman, Phys. Rev. D **15**, 2590 (1977).
[7] A. W. Thomas, Phys. Lett. **126B**, 97 (1983).
[8] J. Speth and A. W. Thomas, in *Advances in Nuclear Physics* (Springer US, Boston, MA, 1997), Vol. 24, pp. 83–149.
[9] A. Szczurek, A. J. Buchmann, and A. Faessler, J. Phys. G **22**, 1741 (1996).
[10] C. Bourrely, J. Soffer, and F. Buccella, Eur. Phys. J. C **23**, 487 (2002).
[11] C. Bourrely and J. Soffer, Nucl. Phys. **A941**, 307 (2015).
[12] S. D. Ellis and W. J. Stirling, Phys. Lett. B **256**, 258 (1991).
[13] A. Baldit *et al.* (NA51 Collaboration), Phys. Lett. B **332**, 244 (1994).
[14] E. A. Hawker *et al.* (FNAL E866/NuSea Collaboration), Phys. Rev. Lett. **80**, 3715 (1998).
[15] J. C. Peng *et al.* (FNAL E866/NuSea Collaboration), Phys. Rev. D **58**, 092004 (1998).
[16] R. S. Towell *et al.* (FNAL E866/NuSea Collaboration), Phys. Rev. D **64**, 052002 (2001).
[17] K. Ackerstaff *et al.* (HERMES Collaboration), Phys. Rev. Lett. **81**, 5519 (1998).
[18] S. Kumano, Phys. Rep. **303**, 183 (1998).
[19] R. Vogt, Prog. Part. Nucl. Phys. **45**, S105 (2000).
[20] G. T. Garvey and J. C. Peng, Prog. Part. Nucl. Phys. **47**, 203 (2001).
[21] W.-C. Chang and J.-C. Peng, Prog. Part. Nucl. Phys. **79**, 95 (2014).

[22] D. F. Geesaman and P. E. Reimer, Rep. Prog. Phys. **82**, 046301 (2019).
[23] C. A. Aidala *et al.* (FNAL E906/SeaQuest Collaboration), Nucl. Instrum. Methods Phys. Res., Sect. A **930**, 49 (2019).
[24] J. Dove *et al.* (FNAL E906/SeaQuest Collaboration), Nature (London) **590**, 561 (2021); **604**, E26 (2022).
[25] J. Dove *et al.* (FNAL E906/SeaQuest Collaboration), Phys. Rev. C **108**, 035202 (2023).
[26] C. H. Leung *et al.* (FNAL E906/SeaQuest Collaboration), Phys. Lett. B **858**, 139032 (2024).
[27] C. Cocuzza, W. Melnitchouk, A. Metz, and N. Sato (Jefferson Lab Angular Momentum (JAM) Collaboration), Phys. Rev. D **104**, 074031 (2021).
[28] R. D. Ball *et al.* (NNPDF Collaboration), Eur. Phys. J. C **82**, 428 (2022).
[29] A. Accardi, X. Jing, J. F. Owens, and S. Park, Phys. Rev. D **107**, 113005 (2023).
[30] S. Alekhin, M. V. Garzelli, S. Kulagin, and S.-O. Moch, Eur. Phys. J. C **83**, 829 (2023).
[31] L. Harland-Lang, T. Cridge, M. Reader, and R. S. Thorne, Eur. Phys. J. C **86**, 115 (2026).
[32] J. Adam *et al.* (STAR Collaboration), Phys. Rev. D **103**, 012001 (2021).
[33] J. Soffer and C. Bourrely, Nucl. Phys. **A991**, 121607 (2019).
[34] M. Alberg, L. Ehinger, and G. A. Miller, Phys. Rev. D **105**, 114054 (2022).
[35] L. Chang, F. Gao, and C. D. Roberts, Phys. Lett. B **829**, 137078 (2022).
[36] P.-L. Yin, Y.-Z. Xu, Z.-F. Cui, C. D. Roberts, and J. Rodríguez-Quintero, Chin. Phys. Lett. **40**, 091201 (2023).
[37] S. D. Drell and T.-M. Yan, Phys. Rev. Lett. **25**, 316 (1970); **25**, 902(E) (1970).
[38] P. J. Ehlers, A. Accardi, L. T. Brady, and W. Melnitchouk, Phys. Rev. D **90**, 014010 (2014).
[39] J. T. Londergan, J. C. Peng, and A. W. Thomas, Rev. Mod. Phys. **82**, 2009 (2010).
[40] R. E. Kalman, J. Basic Eng. **82**, 35 (1960).
[41] S. Agostinelli *et al.* (GEANT4 Collaboration), Nucl. Instrum. Methods Phys. Res., Sect. A **506**, 250 (2003).
[42] J. Allison *et al.*, IEEE Trans. Nucl. Sci. **53**, 270 (2006).
[43] J. Allison *et al.*, Nucl. Instrum. Methods Phys. Res., Sect. A **835**, 186 (2016).
[44] T.-J. Hou, S. Dulat, J. Gao, M. Guzzi, J. Huston, P. Nadolsky, C. Schmidt, J. Winter, K. Xie, and C.-P. Yuan, J. High Energy Phys. 02 (2018) 059.
[45] S. Prasad, Measurement of high-mass dimuon production for $p+p$ and $p+d$ collisions with 120 GeV proton beam at Fermilab, Ph.D. thesis, University of Illinois at Urbana-Champaign, 2020.
[46] C. H. Leung, Probing parton distributions in proton using Drell-Yan and charmonium production in $p+p$ and $p+d$ interactions with 120 GeV proton beam at Fermilab, Ph.D. thesis, University of Illinois at Urbana-Champaign, 2024.
[47] J. Dove, Probing the flavor dependence of proton's light-quark sea in the SeaQuest experiment at Fermilab, Ph.D. thesis, University of Illinois at Urbana-Champaign, 2020.
[48] R. Barlow and C. Beeston, Comput. Phys. Commun. **77**, 219 (1993).
[49] S. F. Pate *et al.* (FNAL E906/SeaQuest Collaboration), J. Instrum. **18**, P10032 (2023).
[50] S. Camarda *et al.*, Eur. Phys. J. C **80**, 251 (2020); **80**, 440(E) (2020).
[51] M. Constantinou *et al.*, Prog. Part. Nucl. Phys. **121**, 103908 (2021).
[52] C. H. Leung *et al.* (FNAL E906/SeaQuest Collaboration), Final SeaQuest results on the flavor asymmetry of the proton light-quark sea with proton-induced Drell-Yan process, HEPData (collection), 2025, https://www.hepdata.net/record/169069.

End Matter

The measured $\sigma_{pd}/2\sigma_{pp}$ cross section ratios are also shown as functions of x_1 and x_F in Fig. 4 and compared with NLO calculations using CJ22 [29] and NNPDF4.0 [28]. The results are tabulated in

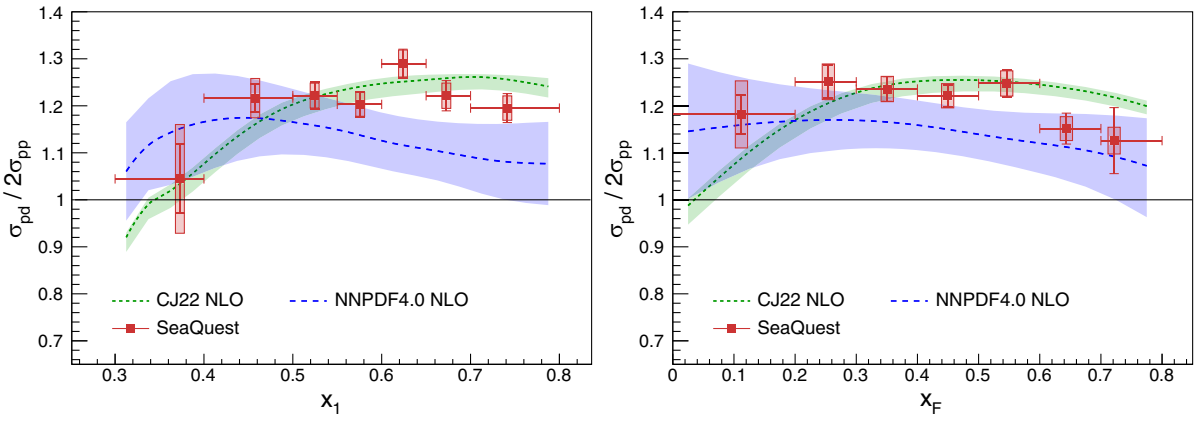

FIG. 4. Measured $\sigma_{pd}/2\sigma_{pp}$ Drell-Yan cross section ratio as functions of x_1 (left) and x_F (right) from SeaQuest compared calculations using CJ22 [29] and NNPDF4.0 [28]. The error bands on the theoretical calculations correspond to the 68% confidence level from the PDFs.

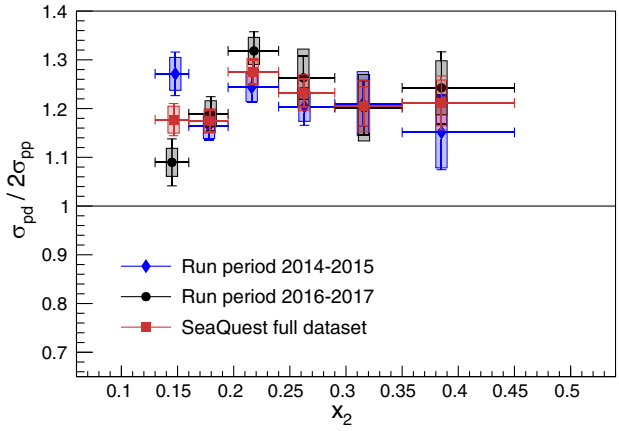

FIG. 5. Comparison of the measured $\sigma_{pd}/2\sigma_{pp}$ ratios as functions of x_2 from the different run periods: 2014–2015 (blue diamonds), 2016–2017 (black circles), and the combined result (red squares).

TABLE III. Measured $\sigma_{pd}/2\sigma_{pp}$ cross section ratio as functions of x_1 and x_F. The first uncertainty is statistical, and the second is systematic.

x_1 range	$\langle x_1 \rangle$	$\langle p_T \rangle$ (GeV/c)	$\langle M \rangle$ (GeV/c^2)	$\sigma_{pd}/2\sigma_{pp}$	x_F range	$\langle x_F \rangle$	$\langle p_T \rangle$ (GeV/c)	$\langle M \rangle$ (GeV/c^2)	$\sigma_{pd}/2\sigma_{pp}$
0.30–0.40	0.373	0.697	5.16	$1.045 \pm 0.074 \pm 0.116$	−0.10–0.20	0.112	0.771	5.50	$1.182 \pm 0.042 \pm 0.071$
0.40–0.50	0.458	0.759	5.19	$1.216 \pm 0.030 \pm 0.042$	0.20–0.30	0.254	0.779	5.27	$1.251 \pm 0.035 \pm 0.038$
0.50–0.55	0.525	0.765	5.21	$1.222 \pm 0.028 \pm 0.026$	0.30–0.40	0.351	0.777	5.20	$1.236 \pm 0.026 \pm 0.027$
0.55–0.60	0.576	0.764	5.24	$1.203 \pm 0.026 \pm 0.025$	0.40–0.50	0.449	0.772	5.18	$1.221 \pm 0.024 \pm 0.026$
0.60–0.65	0.624	0.764	5.28	$1.290 \pm 0.030 \pm 0.029$	0.50–0.60	0.546	0.766	5.17	$1.248 \pm 0.028 \pm 0.027$
0.65–0.70	0.673	0.763	5.32	$1.221 \pm 0.032 \pm 0.027$	0.60–0.70	0.644	0.763	5.15	$1.151 \pm 0.033 \pm 0.025$
0.70–0.80	0.741	0.761	5.36	$1.195 \pm 0.031 \pm 0.026$	0.70–0.80	0.722	0.761	4.95	$1.126 \pm 0.070 \pm 0.028$

TABLE IV. Acceptance of the spectrometer for different x_1 and x_2 bins. In each cell, the first value is the acceptance, the second is the average x_1, the third is the average x_2, and the fourth is the average mass in GeV/c^2.

	x_1									
x_2	0.30–0.35	0.35–0.40	0.40–0.45	0.45–0.50	0.50–0.55	0.55–0.60	0.60–0.65	0.65–0.70	0.70–0.75	0.75–0.80
0.130–0.160						1.19% 0.590 0.157 4.54	2.47% 0.628 0.153 4.60	3.22% 0.676 0.148 4.67	3.81% 0.723 0.144 4.77	4.35% 0.772 0.143 4.91
0.160–0.195				1.03% 0.489 0.191 4.55	1.97% 0.529 0.184 4.63	2.66% 0.575 0.178 4.73	3.64% 0.623 0.176 4.89	4.08% 0.673 0.176 5.08	4.87% 0.722 0.176 5.27	5.40% 0.771 0.175 5.44
0.195–0.240		0.04% 0.393 0.235 4.54	0.66% 0.433 0.226 4.64	1.51% 0.476 0.218 4.77	2.50% 0.524 0.215 4.97	3.34% 0.574 0.215 5.20	4.32% 0.623 0.215 5.42	5.08% 0.673 0.215 5.64	5.65% 0.723 0.215 5.85	6.06% 0.771 0.214 6.02
0.240–0.290	0.03% 0.343 0.279 4.63	0.26% 0.383 0.267 4.76	0.95% 0.427 0.264 4.97	2.02% 0.474 0.263 5.23	3.00% 0.524 0.261 5.49	4.03% 0.574 0.262 5.76	4.92% 0.623 0.262 6.00	5.56% 0.673 0.262 6.23	6.11% 0.722 0.262 6.46	6.32% 0.771 0.262 6.68

(Table continued)

TABLE IV. *(Continued)*

	x_1									
x_2	0.30–0.35	0.35–0.40	0.40–0.45	0.45–0.50	0.50–0.55	0.55–0.60	0.60–0.65	0.65–0.70	0.70–0.75	0.75–0.80
0.290–0.350	0.04%	0.45%	1.38%	2.46%	3.40%	4.18%	5.02%	5.50%	6.19%	6.10%
	0.338	0.379	0.425	0.474	0.524	0.573	0.624	0.673	0.722	0.772
	0.323	0.318	0.316	0.315	0.316	0.315	0.314	0.314	0.313	0.315
	4.92	5.16	5.44	5.75	6.04	6.32	6.59	6.84	7.09	7.36
0.350–0.450	0.08%	0.64%	1.48%	2.32%	3.09%	3.80%	4.37%	4.68%	4.93%	4.85%
	0.337	0.377	0.425	0.475	0.523	0.573	0.624	0.671	0.721	0.772
	0.385	0.387	0.386	0.385	0.385	0.384	0.383	0.379	0.380	0.378
	5.38	5.69	6.03	6.38	6.69	6.99	7.29	7.53	7.81	8.06

Table III. To compare theoretical calculations with the cross section ratios presented in Figs. 2 and 4, the calculations are weighted by the spectrometer acceptance, tabulated in Table IV. The comparison of the measured $\sigma_{pd}/2\sigma_{pp}$ ratios as functions of x_2 from the different run periods is shown in Fig. 5.